

Supporting Information

Title: Multifunctional carbon-supported bioactive hybrid nanocomposite (C/GO/NCP) bed for the superior water decontamination from waterborne microorganisms

Michał Jakubczak^{1, a, *}, *Ewa Karwowska*^{2, b}, *Alicja Fiedorczuk*^{2, c}, and *Agnieszka M. Jastrzębska*^{1, d}

¹ Warsaw University of Technology, Faculty of Materials Science and Engineering, Woloska 141, 02-507 Warsaw, Poland

² Warsaw University of Technology, Faculty of Building Services, Hydro and Environmental Engineering, Nowowiejska 20, 00-653 Warsaw, Poland

^a michal.jakubczak.dokt@pw.edu.pl

^b ewa.karwowska@pw.edu.pl

^c ala.fiedorczuk@gmail.com

^d agnieszka.jastrzebska@pw.edu.pl

***Corresponding Authors. Email:** Mr. Michał Jakubczak, michal.jakubczak.dokt@pw.edu.pl, +48-22-234-7449

S.1 Characterization of the granular activated carbon (C)



Figure S1.1 Photograph of the pristine granular activated carbon (C) used as macroscopic supporting material for bioactive hybrid nanocomposite particles.

Preliminary characterization of the C morphology was carried out using ECLIPSE MA 200 metallographic microscope. Microscopic images revealed numerous cracks and pores in C grains (**Fig. S1.2**). One can also notice some textural arrangement of longitudinal capillary pores in various areas of the investigated C sample.

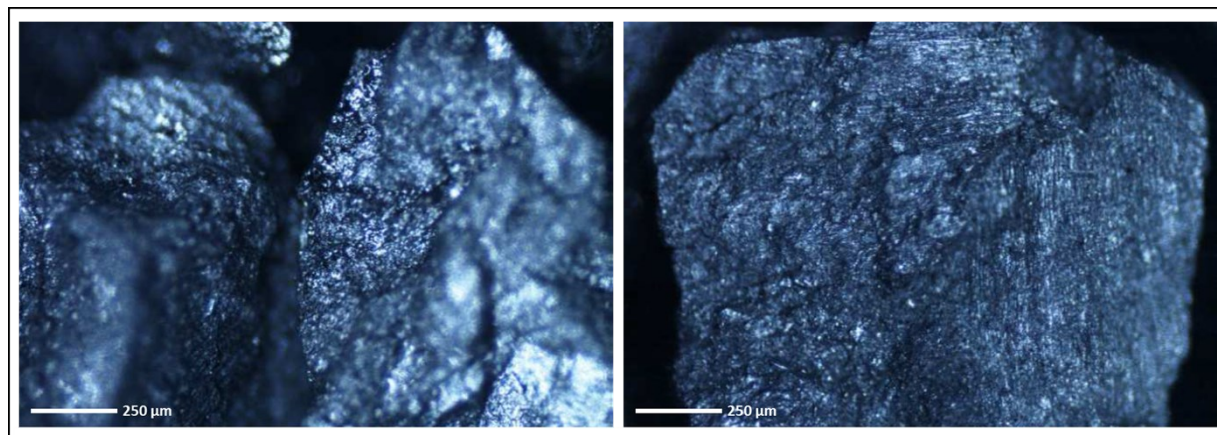


Figure S1.2 The set of microscopic images obtained for the pristine granular activated carbon (C).

Detailed morphology studies of the C sample were carried out using LEO 1530 (Zeiss, USA) scanning electron microscope at an acceleration voltage of 2.0 kV. For SEM observations, randomly selected grains of C sample were placed onto the surface of sticky carbon tape. Samples were then sputtered with a thin layer of carbon using a BAL-TEC SCD 005 sputter coater. The SEM analysis of G grains (**Fig. S.1.3**) showed large porosity and heterogeneous morphology. One could also observe numerous longitudinal capillaries related to the anisotropy of the observed structure.

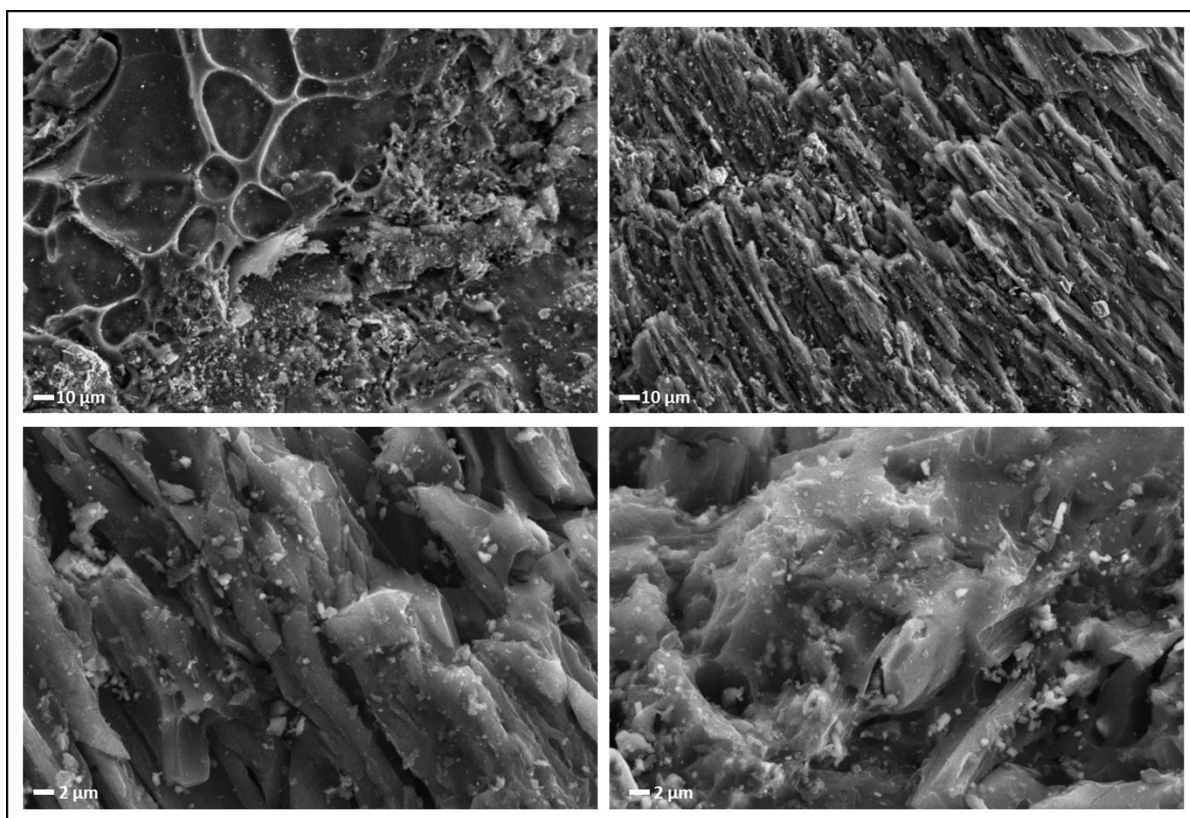


Figure S1.3 The set of SEM images obtained for the granular activated carbon (C).

The physical properties of C grains were analyzed using the nitrogen sorption technique. Adsorption and desorption of the nitrogen from C surface was carried out using Quadrasorb-SI (Quantachrome Instruments, Germany) in a liquid nitrogen bath at $-195\text{ }^{\circ}\text{C}$.

To determine the sample's specific surface area (S_{BET}), we have applied the Brunauer-Emmett-Teller (BET) calculation method. At the same time, the total pore volume (V_{pore}) and average pore size (D_{pore}) were analyzed using Barret-Joyner-Halend (BJH) method.

The obtained results indicate that with a relatively high total pore volume ($0.047 \text{ cm}^3 \text{ g}^{-1}$), the specific surface area of the tested carbon was $796.6 \text{ m}^2 \text{ g}^{-1}$. At the same time, the average pore size for C grains was approximately 3 nm.

Table S.1.1 Physical properties of granular activated carbon (C) grains such as Brunauer-Emmett-Teller surface area (S_{BET}), total pore volume (V_{pore}), and mean pore size (D_{pore}), obtained using physical nitrogen sorption analysis.

Sample	S_{BET} ($\text{m}^2 \text{ g}^{-1}$)	V_{pore} ($\text{cm}^3 \text{ g}^{-1}$)	D_{pore} (nm)
Granular activated carbon	796.6	0.047	3

Studies of antibacterial properties were carried out as follows: sterile, wet paper discs (within 0.6 centimeters diameter) were dip into the powdered sample. The sample was then studied using the disc diffusion method and *Bacillus mycoides*, *Bacillus sp.* and *Staphylococcus sp.* bacteria strains, obtained from the private collection of the Biology Department, Faculty of Building Services, Hydro and Environmental Engineering, Warsaw University of Technology. Samples were cultured using Petri plates on the surface of nutritive agar medium (Merck, USA) in Petri dishes for 24 hours at 26°C (*Bacillus mycoides*, *Bacillus sp.*) or 37°C (*Staphylococcus sp.*).

The results indicate that C grains did not possess antibacterial properties against investigated strains. Growth inhibition zones were not detected.

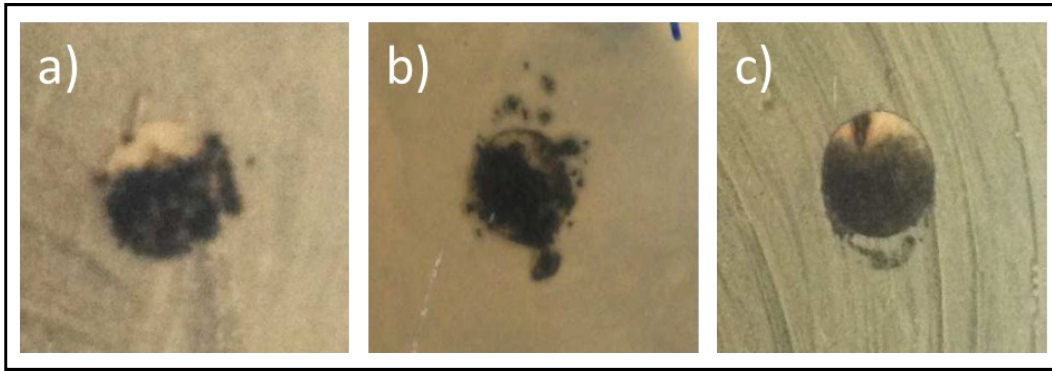


Figure S.1.4 Photographs of Petri plates showing the results of disc diffusion test in presence of the pristine granular activated carbon (C) grains: **a)** *Bacillus mycoides*, **b)** *Bacillus sp.* and **c)** *Staphylococcus sp.*

S.2 Characterization of the C/Al₂O₃/Ag hybrid nanocomposite (C/NCP)

Morphology of C/NCP was studied using LEO 1530 (Zeiss, USA) scanning electron microscope (SEM) operating at an acceleration voltage of 2 kV. Secondary electron (SE) and Energy Selective Backscattered (ESB) detectors were used to identify Al₂O₃ and Ag nanoparticles decorating the C surface. An analysis of the elemental composition was carried out using the Energy Dispersive X-ray Spectroscopy (EDS) technique.

The SEM analysis revealed that the surface of C was covered by Al₂O₃/Ag hybrid nanometric-sized composite particles. These grains were unevenly distributed and formed agglomerates of different sizes. Also, the SEM-ESB analysis allowed us to observe individual Ag nanoparticles revealed here as bright spots.

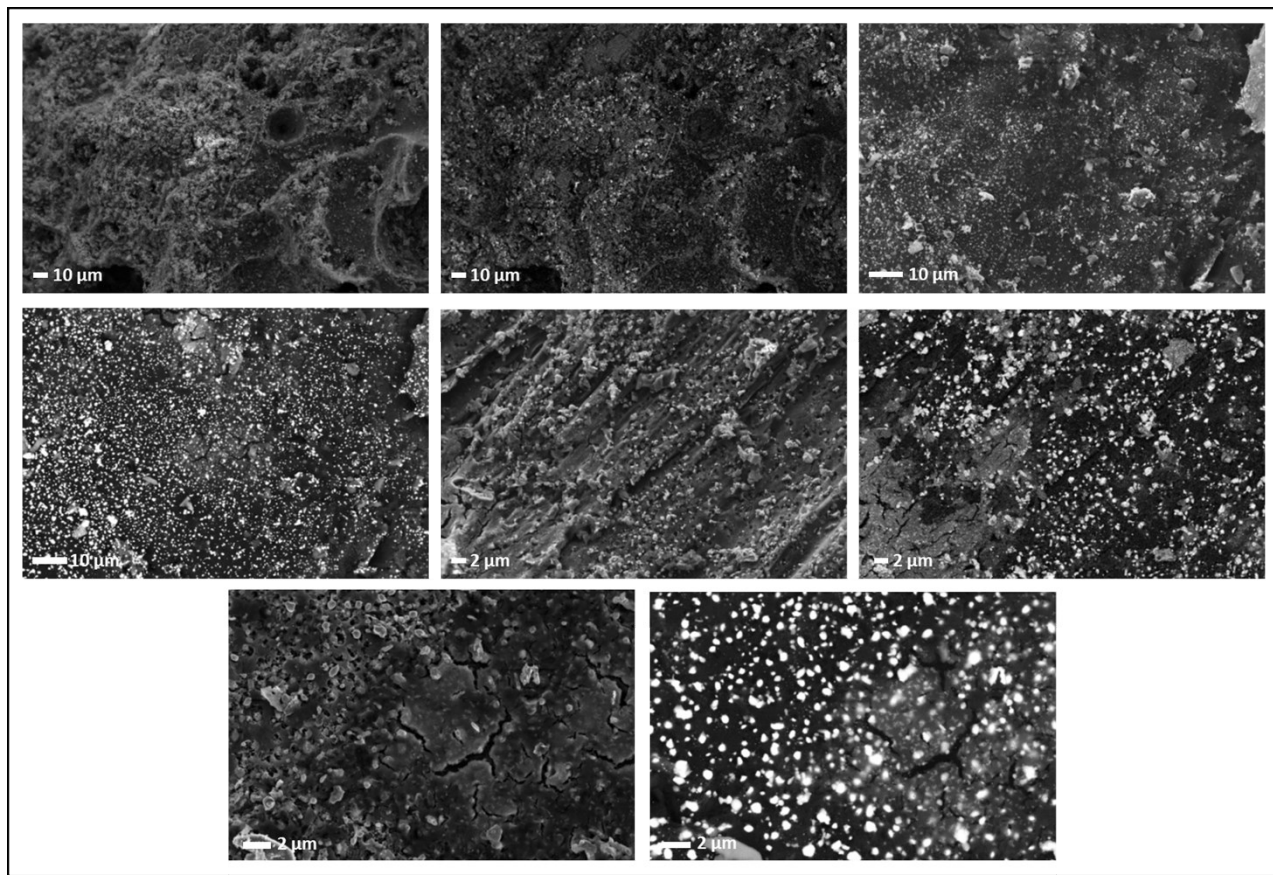


Figure S.2.1 The set of SEM images obtained for the C/Al₂O₃/Ag hybrid nanocomposite (C/NCP).

Results of the SEM-EDS analysis for C/NCP hybrid nanocomposite were presented in **Fig. S.2.2**. EDS spectrum was obtained for the selected analysis area, marked in **Fig. S.2.2a**. The EDS spectrum showed the presence of aluminum (Al), oxygen (O), and silver (Ag) as well as the compositional elements of the Al₂O₃/Ag, as well as carbon (C), sulfur (S), and silicon (Si). The obtained results confirmed that brighter spots observed in **Fig. S.2.1** are NCP, deposited on the carbon surface, while the presence of sulfur and silicon indicates contamination of granular activated carbon.

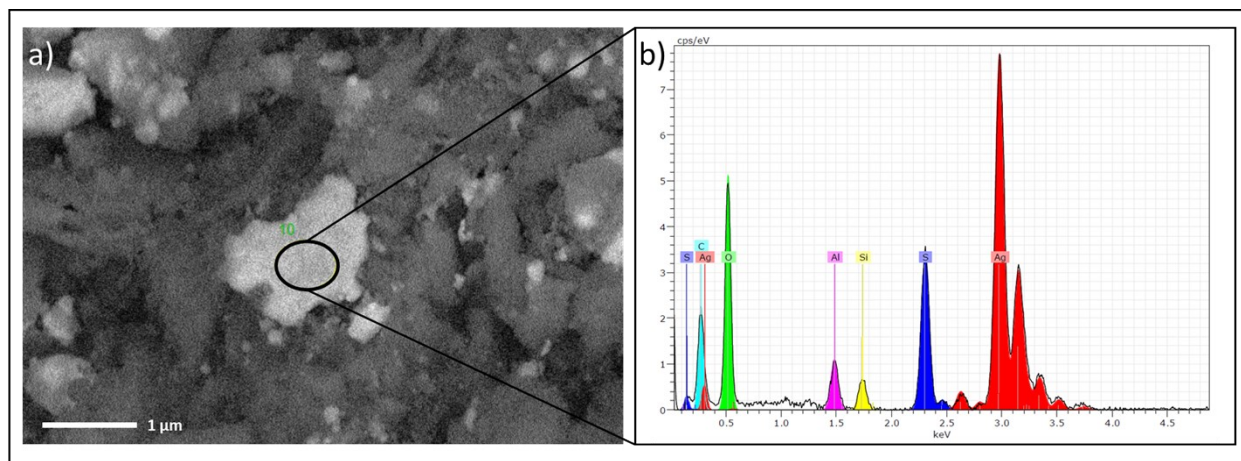


Figure S.2.2 Results of the EDS analysis of C/Al₂O₃/Ag hybrid nanocomposite (C/NCP): **a)** the analyzed area of the sample and **b)** obtained EDS spectrum.

EDS mapping of the C/Al₂O₃/Ag hybrid nanocomposite composition additionally confirmed the presence of Al₂O₃/Ag NCP covering the surface of granular activated carbon. It could also be observed that, in case of larger clusters, Al was a dominating element over Ag presence. Therefore, the agglomerates were a result of Al₂O₃ agglomeration, not the Ag agglomeration.

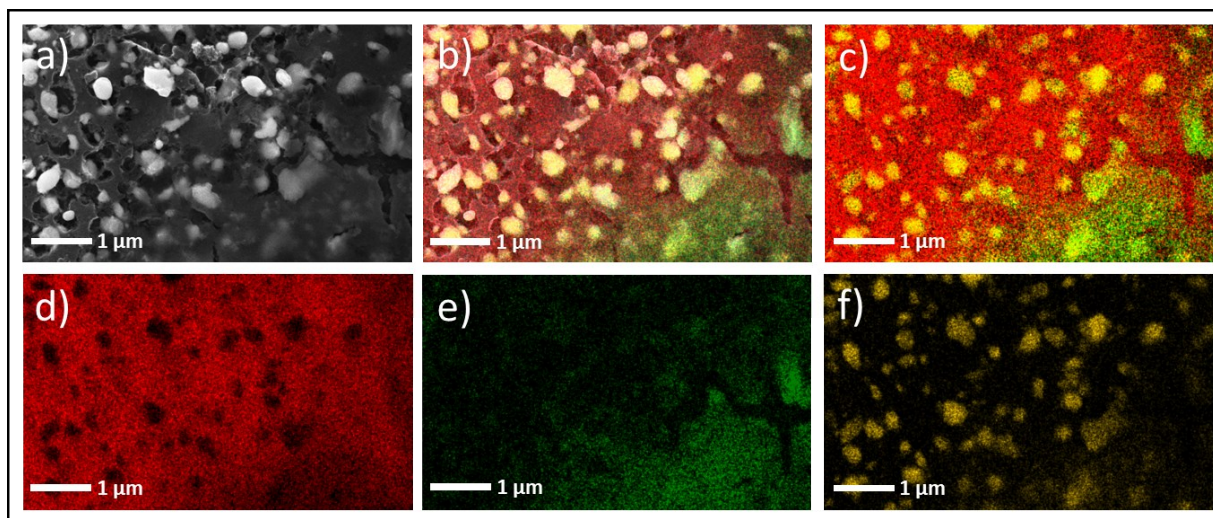


Figure S.2.3 The EDS mapping of the $C/Al_2O_3/Ag$ hybrid nanocomposite (C/NCP) showing an elemental composition in the frame of **a)** the whole analyzed area; **b)** mixed-signal from C, Al, Ag; **c)** mixed-signal from Al, Ag; **d)** signal form only C; **e)** signal form only Al; **f)** signal form only Ag.

The physical properties of C/NCP were studied using the nitrogen sorption method. We have used the same approach as in case of C sample. The results were summarized in **Tab. S.2.1**. As one could notice, decoration of the surface of C grains with NCP resulted in a slight reduction of specific surface area (by about $34 \text{ m}^2 \text{ g}^{-1}$) and an increase in total pore volume and average pore size.

Table S.2.1 Physical properties of $C/Al_2O_3/Ag$ hybrid nanocomposite (C/NCP) such as Brunauer-Emmett-Teller surface area (S_{BET}), pore volume (V_{pore}), and mean pore size (D_{pore}), obtained using physical nitrogen sorption analysis.

Sample	$S_{BET} (\text{m}^2 \text{ g}^{-1})$	$V_{pore} (\text{cm}^3 \text{ g}^{-1})$	$D_{pore} (\text{nm})$
$C/Al_2O_3/Ag$	1006.1	0.107	3

Antibacterial properties of C/Al₂O₃/Ag hybrid nanocomposite were studied using the disc diffusion method, using the same approach as in case of C sample. The obtained results indicate that modification of granular activated carbon with NCP resulted in the appearance of biocidal activity against investigated bacteria strains. The strongest antibacterial activity was observed for *Bacillus sp.*, *Sarcina sp.* and *Staphylococcus sp.* strains.

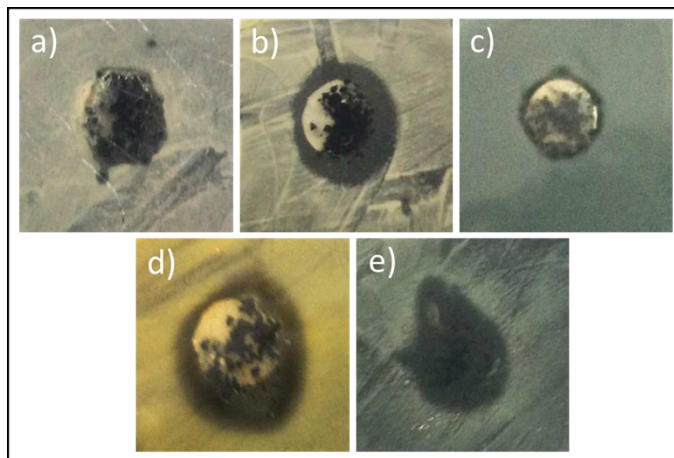


Figure S.2.4 Photographs of Petri plates showing the results of disc diffusion test in presence of the C/Al₂O₃/Ag hybrid nanocomposite (C/NCP): **a)** *Bacillus mycoides*, **b)** *Bacillus sp.*, **c)** *E. coli*, **d)** *Sarcina sp.* and **e)** *Staphylococcus sp.*

SEM images of the C/NCP with adsorbed *coccobacillus* and *staphylococci* bacteria cells mix revealed that both types of bacteria cells were readily adsorbed on the surface of investigated hybrid nanocomposite. Large groups of cells were observed mainly at the edges and in larger pores of the studied material. The larger cell clusters consisted mainly of cells with the same morphology. We did not notice the bacteria cells avoiding stacking in areas rich in the introduced nanocomposite (lighter dots) or having abnormalities in their morphology.

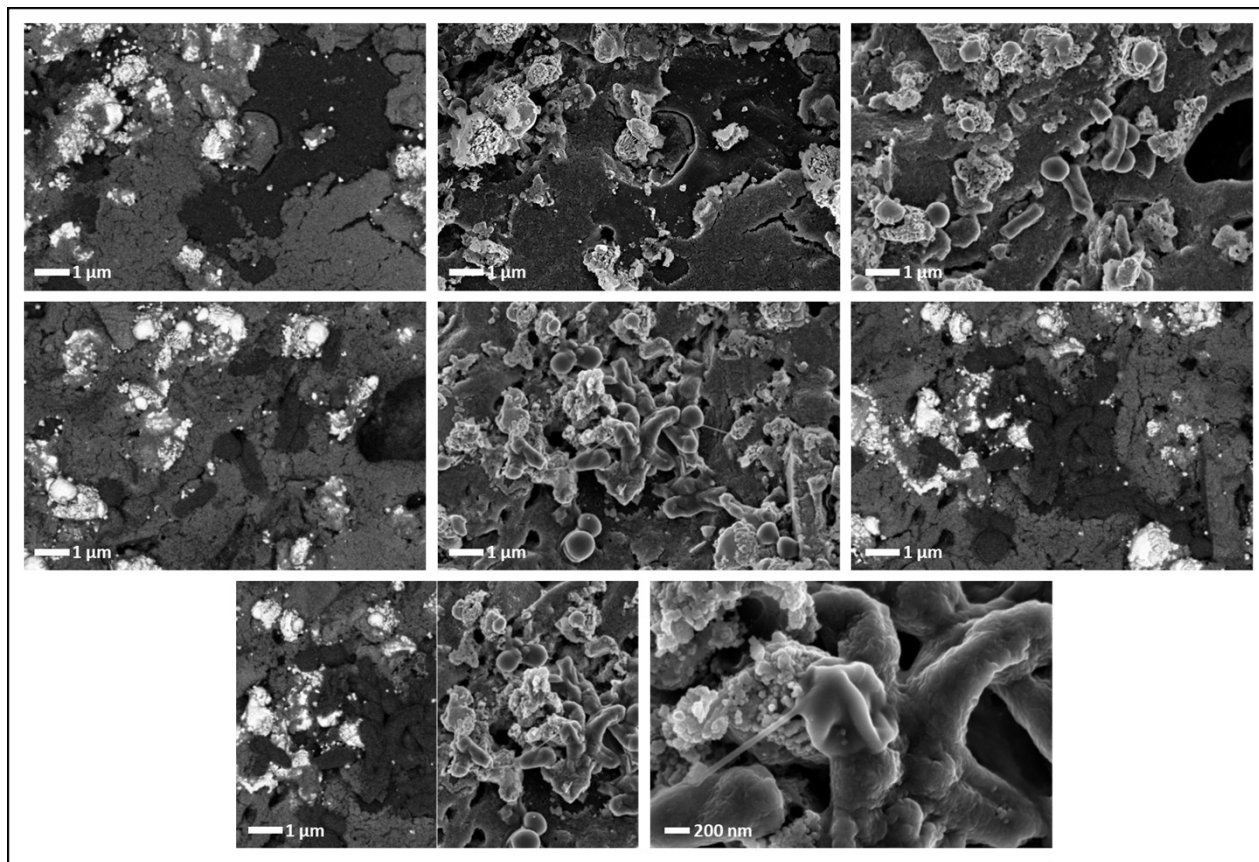


Figure S.2.5 SEM images for C/Al₂O₃/Ag hybrid nanocomposite (C/NCP) with adsorbed *coccobacillus* and *staphylococci* bacteria cells mix.

S.3 Characterization of the C/GO/Al₂O₃/Ag hybrid nanocomposite (C/GO/NCP)

The SEM images obtained for C/GO/NCP hybrid nanocomposite (**Fig. S.3.1**) revealed that the surface of supporting C grains was covered with micrometric-scale flakes of heterogeneous morphology and shape. Those extra flakes were unevenly distributed and formed individual GO/NCP structures. The SEM-BSE analysis showed that Al₂O₃/Ag nanoparticles (NCP) are present on both GO surface and C grains. These can be easily seen as brighter points on SEM-BSE images.

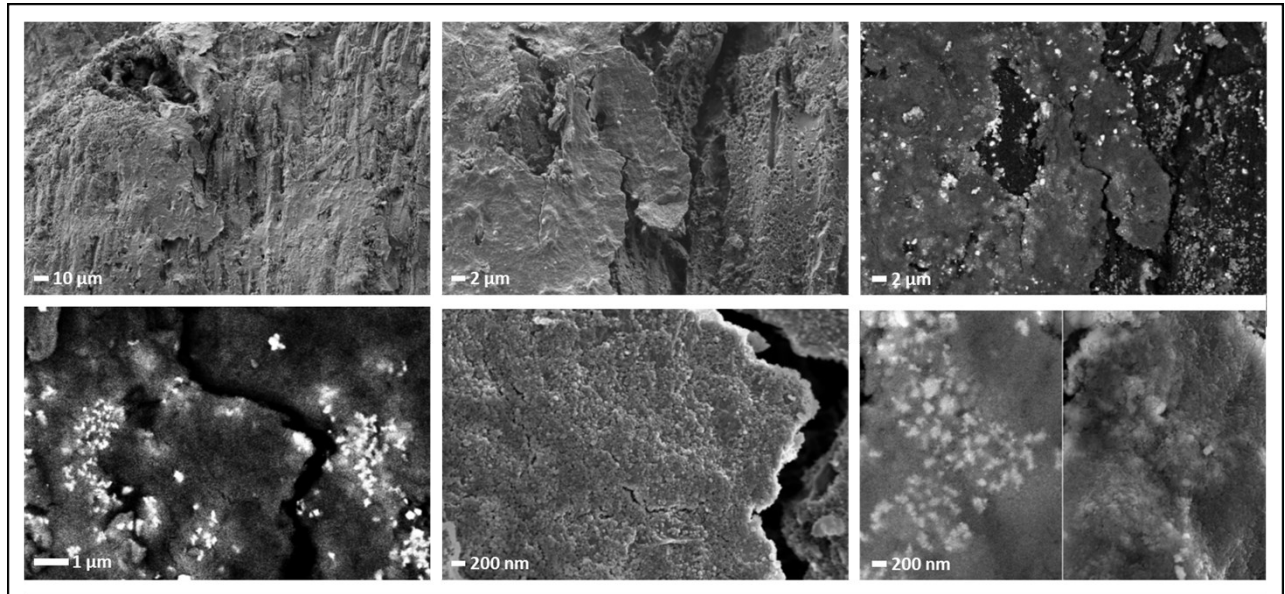


Figure S.3.1 The set of SEM images obtained for the C/GO/Al₂O₃/Ag hybrid nanocomposite (C/GO/NCP).

The SEM images obtained for the C/GO/NCP with adsorbed *coccobacillus* and *staphylococci* bacteria cells mix revealed that bacteria cells adsorbed mostly on the surface of pores of the investigated hybrid nanocomposite structure. The larger cell clusters were also present here and were formed by cells of the same morphology. Even though the morphology of bacteria cells was not changed in most cases, some *coccobacillus* cells seem to possess cylindrical, recessed shapes. What is more, the SEM-BSE imaging revealed that some *staphylococcus* cells were bright, while the others were dark, which could be due to the I₂O₃/Ag uptake.

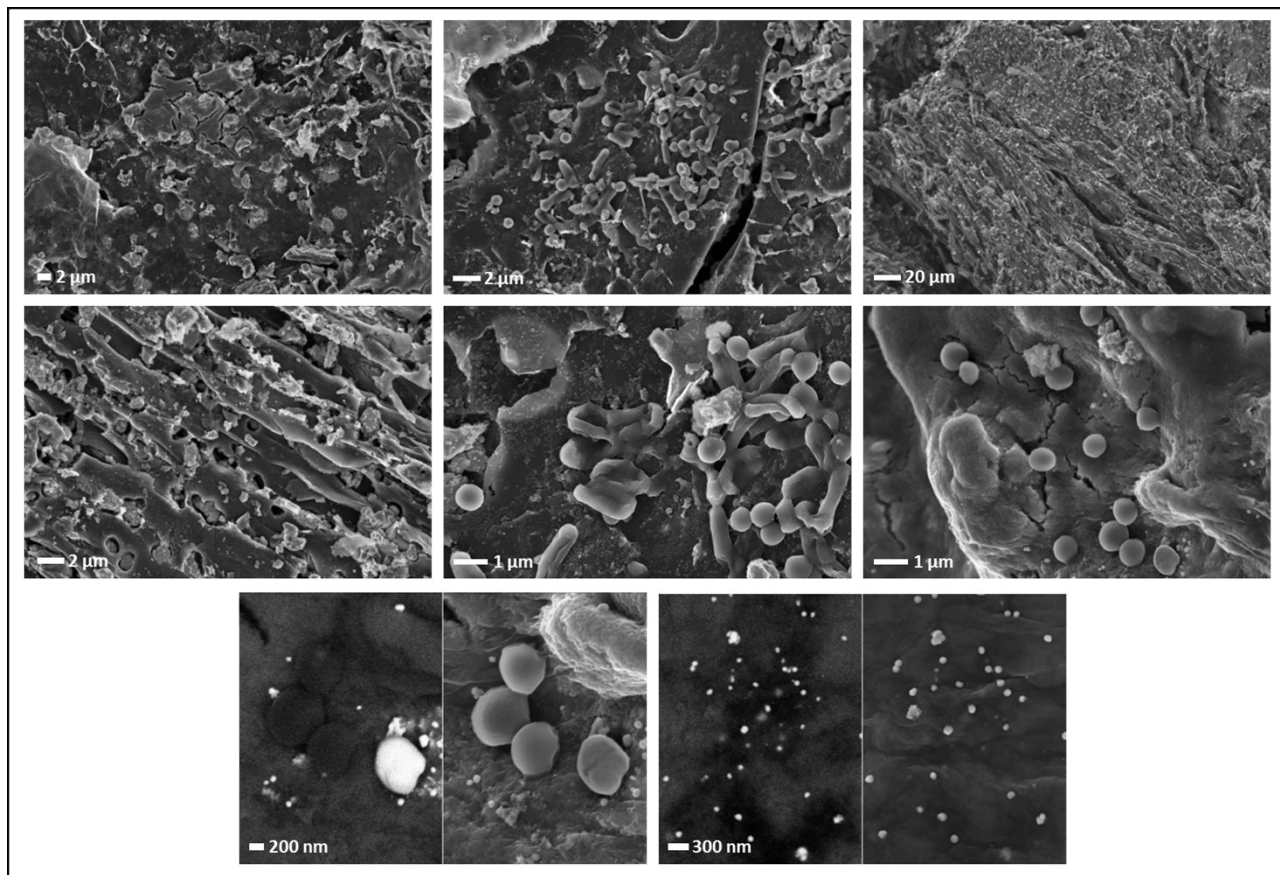


Figure S.3.2 SEM images of the C/GO/Al₂O₃/Ag hybrid nanocomposite (C/GO/NCP) with adsorbed *coccobacillus* and *staphylococci* bacteria cells mix.

S.4 Waterborne bacteria

Waterborne bacteria strains were isolated from the natural (real) water samples collected in Poland, from water ditch (**Fig. S.4.1**), located in a small town (less than 20 000 inhabitants), near the ‘S7’ highway (Grójec, Poland, 51°51'17.5"N 20°51'57.0"E). Water samples were collected from the depth of 10 cm using sterile containers, which were then stored at 4 °C.



Figure S.4.1 Area of water sampling.

Bacteria strains were isolated from the collected water samples (**Fig. S.4.2**) using the streaking technique and then characterized in terms of morphology and Gram staining. As summarized in **Tab. S.4.1**, we have isolated two *Pseudomonas sp.*, *Bacillus sp.*, *Sarcina sp.*, *Pseudomonas fluorescens*, and *Staphylococcus sp.*. From all of the isolated bacteria, there were three Gram-positive and three Gram-negative strains. The Gram staining of (*W4*) did not reveal any information because of its poor growth and not fully clear morphology.

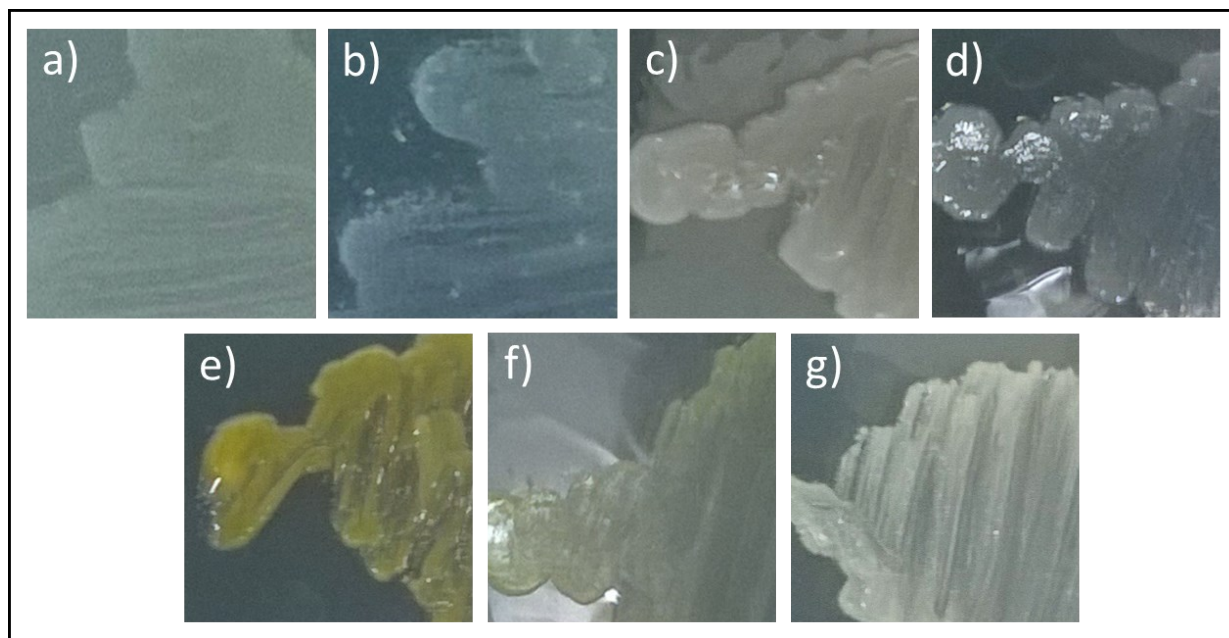


Figure S.4.2 Waterborne bacterial strains isolated from the samples of natural surface water: a) W3, b) W4, c) W6, d) W7, e) W8, f) W9, g) W12.

Table S.4.1 Description of waterborne bacteria strains.

Bacteria	Strain	Gram stain
<i>W3</i>	<i>Pseudomonas sp.</i>	-
<i>W4</i>	<i>poorly growing strain</i>	not clear
<i>W6</i>	<i>Bacillus sp.</i>	+
<i>W7</i>	<i>Pseudomonas sp.</i>	-
<i>W8</i>	<i>Sarcina sp.</i>	+
<i>W9</i>	<i>Pseudomonas fluorescens</i>	-
<i>W12</i>	<i>Staphylococcus sp.</i>	+

S.5 Filtration process

Experimental filtration setup was presented in **Fig. S.5.1**. It was created using columns of the 20 cm volumetric capacity and 1 cm diameter, which were mounted to the stabilizing frame. We have introduced the C/NCP and C/GO/NCP to each column to form a bed with 10 cm high.

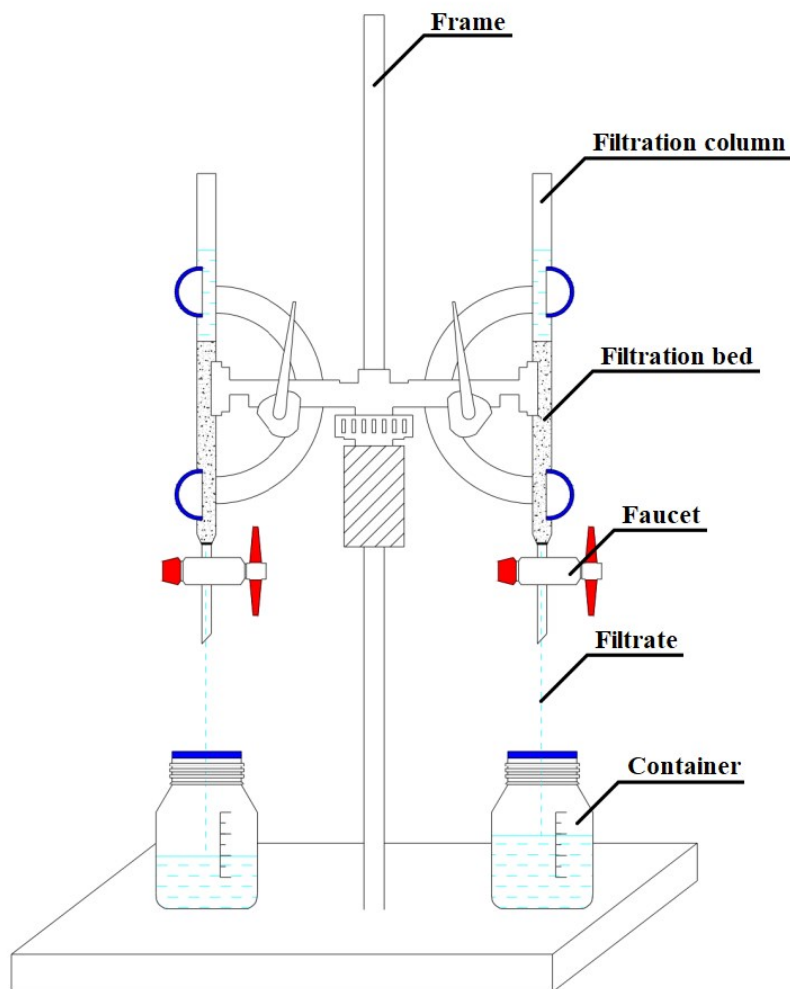


Figure S.5.1 Experimental setup for the filtration approach used in this study.

S.6 Summary of biocidal properties of the obtained materials against waterborne bacteria strains

Antibacterial properties of granular activated carbon grains (C), as well as C/Al₂O₃/Ag (C/NCP) and C/GO/Al₂O₃/Ag (C/GO/NCP) hybrid nanocomposites, were summarized in **Tab. S.6.1**. In most cases, C/NCP nanocomposite exhibited a slightly better antibacterial activity than C/GO/NCP. Abnormalities were observed only in case of *W12* bacteria, which formed a growth inhibition zone, that was almost three times bigger in case of nanocomposite lacking GO addition. *W4*, *W6* and *W9* bacteria strains were characterized by complete resistance to investigated hybrid nanocomposites.

Tab. S.6.1 Summary of the antibacterial properties of the pristine activated carbon grains (C) (reference sample) as well as C/Al₂O₃/Ag (C/NCP) and C/GO/Al₂O₃/Ag (C/GO/NCP) hybrid nanocomposites.

Bacteria strain	Reference sample	C/Al ₂ O ₃ /Ag	C/GO/Al ₂ O ₃ /Ag
W3	0.00 ± 0.00	0.45 ± 0.07	0.30 ± 0.10
W4	0.00 ± 0.00	0.00 ± 0.00	0.00 ± 0.00
W6	0.00 ± 0.00	0.00 ± 0.00	0.00 ± 0.00
W7	0.00 ± 0.00	1.60 ± 0.32	1.52 ± 0.11
W8	0.00 ± 0.00	1.46 ± 0.33	1.18 ± 0.21
W9	0.00 ± 0.00	0.00 ± 0.00	0.00 ± 0.00
W12	0.00 ± 0.00	3.08 ± 0.64	1.13 ± 0.30

The calculated percentage efficiency of the filtration process in eliminating bacterial cells for the hybrid nanocomposites and the regenerated samples was summarized in **Tab. S.6.2**. At

each of the measured points, both hybrid nanocomposites act superior over granular reference carbon. In both cases, for the first 60 minutes of the process, the efficiency was over 99.9%, while in the next 60 minutes it was reduced slightly, but still measuring over 99%. The high efficiency in bacterial cell removal was also maintained after thermal regeneration and in the case of C/Al₂O₃/Ag hybrid nanocomposite over 99.9% for the whole duration of the process.

Table S.6.2 The percentage efficiency of the filtration process in eliminating bacterial cells for the hybrid nanocomposites and the regenerated samples.

Time [min]	Reference	C/Al ₂ O ₃ /Ag	C/GO/Al ₂ O ₃ /Ag	C/Al ₂ O ₃ /Ag (R)	C/GO/Al ₂ O ₃ /Ag (R)
15	92.40	99.99	99.99	99.99	99.88
30	91.05	99.99	99.98	99.99	99.94
45	90.54	99.99	99.63	99.99	99.90
60	89.73	99.99	99.94	99.97	99.92
90	86.49	99.72	99.38	99.94	99.86
120	77.37	98.72	99.98	–	–

Calculated percentage efficiency of the pristine hybrid nanocomposite and the regenerated samples in immobilizing adsorbed bacterial cells after 72 h of contact time was presented in **Tab. S.6.3**. A quick look revealed that self-disinfecting properties characterized both hybrid nanocomposites. In the case of granular activated carbon and after a contact time of 72 hours, only c.a. 95% of adsorbed bacterial cells were immobilized, while for both hybrid nanocomposite materials, it was over 99%. What is more, these properties were preserved in case of C/Al₂O₃/Ag nanocomposite after its thermal regeneration.

Table S.6.3 Calculated percentage efficiency of the pristine hybrid nanocomposite and the regenerated samples in immobilizing adsorbed bacterial cells after 72 hours of contact time.

	Sample				
	Reference	C/GO/Al ₂ O ₃ /Ag	C/Al ₂ O ₃ /Ag	C/GO/Al ₂ O ₃ /Ag (R)	C/Al ₂ O ₃ /Ag (R)
[%]	95.03	99.73	99.95	94.92	99.59

S.7 Summary of DLS and zeta potential studies on colloidal samples

The dynamic light scattering (DLS), zeta potential, electrophoretic mobility, and conductivity studies aimed at tracking the potential particle leakage from C/NCP and C/GO/NCP beds into the filtrate using the NANO ZS ZEN 3500 analyzer equipped with a light scattering detector, operating at an angle of 173°. The measurement series were conducted at 25 °C.

The obtained results of particle leakage were presented in **Tab. S.7.1**. The results indicate that in case of C/NCP filtration material, the first particle emission is related to larger agglomerates of ~313 nm that are being detached from the filtration bed during the first flow of water. In case of C/GO/NCP filtration material, ~91 nm particles were detached from the surface. This means that the presence of GO stabilized the hybrid nanocomposite structure, revealed as preventing the detachment of nanoparticle agglomerates. What is interesting, while only pristine C grains were used for the filtration process, nanometric-sized (~10 nm) C particles were detected. Also, all types of particles were leaked only at the beginning of the filtration process. This is the expected effect resulting from large changes in pressure and flow velocities before the process stabilizes on its own. The important information is that after finishing the filtration, we did not observe any particle leakage.

The zeta potential studies, together with the associated data on electrophoretic mobility and conductivity were carried out at the beginning of the filtration process due to monitor water parameters during the first potential emission of particles (see **Tab. S.7.2**). While the water conductivity was not changed, the electrophoretic mobility of released particles as well as resulting zeta potential depended on the type of emission. In case of nanoparticle emission from the C grains, the zeta potential value was reduced to -16.7 mV compared to the bacteria-contaminated water sample, while in case of C/NCP and C/GO/NCP samples, the zeta potential was -8.78 and -13.9 mV, respectively. These changes indicate that particles leaked from the C/GO/NCP sample created a more stable dispersion in the water environment.

Table S.7.1 Potential particle leakage at the beginning and finishing stages of the filtration process. The pristine water and water sample before the filtration process (containing the waterborne bacteria cells) were used here as a reference.

Sample name / process stage	detected particle size	
	Beginning the filtration	Finishing the filtration
water sample before contamination	0 nm	-
contaminated water sample	2780 nm	-
C grains	10 nm	Not detected
C/Al₂O₃/Ag	313 nm	Not detected
C/GO/Al₂O₃/Ag	91 nm	Not detected

Table S.7.2 Zeta potential, electrophoretic mobility, and conductivity analysis carried out at the beginning of the waterborne bacteria filtration process. The pristine water and water sample before the filtration process (containing the waterborne bacteria cells) were used here as a reference.

Sample name	measured parameter		
	zeta potential (mV)	Electrophoretic mobility ($\mu\text{mcm V}^{-1} \text{s}^{-1}$)	Conductivity (mS cm^{-1})
water sample before contamination	0	0	0
contaminated water sample	-3.6	-0.2822	0.716
C grains	-16.7	-1.306	0.715
C/Al ₂ O ₃ /Ag	-8.78	-0.6886	0.697
C/GO/Al ₂ O ₃ /Ag	-13.9	-1.093	0.66

S.8 Comparison of the results obtained and described in the literature

The results obtained in our work have been compared with those described in the literature (see **Tab. S.8.1.**).

Table S.8.1 Comparison of the result obtained and described in the literature.

Nanocomposite filtration material	Adsorption capacity [$\text{m}^2 \text{g}^{-1}$]	Efficiency of pristine material [%]	Efficiency of reused material [%]	Self- sterilizing ability of pristine material [%]	Self- sterilizing ability of reused material [%]	Reference
C/Al ₂ O ₃ /Ag	1006.1	99.99	99.99	99.95	99.59	This work
C/GO/Al ₂ O ₃ /Ag	948.2	99.99	99.94	99.73	94.92	This work
Ag/Wood Composite	-	99.99	99.99	-	-	(Che <i>et al.</i> 2019)

C/Ag	-	>99.9	-	-	-	(Hung <i>et al.</i> 2020)
Paper/Ag	-	99.99	-	-	-	(Dankovich <i>et al.</i> 2011)
Woven fabric/Ag	-	100.00	-	-	-	(Mecha and Pillay 2014)
Clay/Ag	17.94-52.19	100.00	-	-	-	(Oyanedel-Craver and Smith 2008)
Ti ₃ C ₂ /Al ₂ O ₃ /Ag/ Cu-modified polypropylene fabric	-	52.80- 89.09	-	82.28	-	(Jakubczak <i>et al.</i> 2021)
Oxidized- Ti ₃ C ₂ /Al ₂ O ₃ /Ag/ Cu-modified polypropylene fabric	-	71.44- 90.29	-	99.55	-	(Jakubczak <i>et al.</i> 2021)
Activated carbon fiber/Sophora flavescens nanoparticles	-	93.70	-	28	-	(Sim <i>et al.</i> 2014)
C/Ag	-	100.00	-	-	-	(Ahammad <i>et al.</i> 2008)
CSCI@GO/QS	-	95.74	90.00	-	-	(Li <i>et al.</i> 2019)
TiO ₂ /Ti ₃ C ₂ /PVDF	-	70.00	-	>99.00	-	(Rasool <i>et al.</i> 2017)
GO/Ag	-	-	-	86.00	-	(Sun <i>et al.</i> 2015)

S.9 References

- 1 W. Che, Z. Xiao, Z. Wang, J. Li, H. Wang, Y. Wang and Y. Xie, *ACS Sustain. Chem. Eng.*, 2019, **7**, 5134–5141.
- 2 S. T. Hung, Y. N. Chow, H. Zheng and Z. Li, *IOP Conf. Ser. Earth Environ. Sci.*, 2020, **474**, DOI:10.1088/1755-1315/474/5/052077.
- 3 T. A. Dankovich and D. G. Gray, *Environ. Sci. Technol.*, 2011, **45**, 1992–1998.
- 4 C. A. Mecha and V. L. Pillay, *J. Memb. Sci.*, 2014, **458**, 149–156.
- 5 V. A. Oyanedel-Craver and J. A. Smith, *Environ. Sci. Technol.*, 2008, **42**, 927–933.

- 6 M. Jakubczak, E. Karwowska, A. Rozmysłowska-Wojciechowska, M. Petrus, J. Woźniak, J. Mitrzak and A. M. Jastrzębska, *Materials (Basel)*, 2021, **14**, 1–16.
- 7 K. M. Sim, K. H. Kim, G. B. Hwang, S. C. Seo, G. N. Bae and J. H. Jung, *Sci. Total Environ.*, 2014, **493**, 291–297..scitotenv.2014.06.002.
- 8 T. R. Ahammad, S. Z.; Gomes, J.; Sreekrishnan, *J. Chem. Technol. Biotechnol.*, 2008, **83**, 1163–1169.
- 9 X. Li, J. Sun, Y. Che, Y. Lv and F. Liu, *Int. J. Biol. Macromol.*, 2019, **121**, 760–773.
- 10 K. Rasool, K. A. Mahmoud, D. J. Johnson, M. Helal, G. R. Berdiyrov and Y. Gogotsi, *Sci. Rep.*, 2017, **7**, 1–11.
- 11 X. F. Sun, J. Qin, P. F. Xia, B. B. Guo, C. M. Yang, C. Song and S. G. Wang, *Chem. Eng. J.*, 2015, **281**, 53–59.